第 44 卷 第 5 期/2024 年 3 月/光学学报 研究论文

光学学报

模分复用系统中的CPR-MIMO-CMA研究

杨步高[1]，田凤[1*]，刘小东[2]

[1]北京邮电大学电子工程学院，信息光子学与光通信国家重点实验室，天地互联与融合北京市重点实验室，北京 100876；
[2]北京安科慧生科技有限公司，北京 101102

摘要 针对模分复用系统中由于模式耦合引入的信道串扰(XT)的问题，提出一种基于信号相关峰提取的XT相关比测量方法，并将XT相关系数应用于多进多出恒模盲均衡算法(CPR-MIMO-CMA)中以提升信道均衡效果。搭建了少模光纤传输的实验平台，利用CPR-MIMO-CMA对接收端数据进行处理，研究结果表明，在满足前向纠错(FEC)为3.8×10^{-3}的门限下，所提出的CPR-MIMO-CMA在LP01、LP11、LP21三模信道中比传统CMA分别具有1.3 dB、0.9 dB、1.0 dB的性能增益，并且3个模式下的平均收敛时间减少约50%。

关键词 光通信；模分复用；模间串扰；信号相关峰；模式均衡

中图分类号 TN913.7 **文献标志码** A **DOI**：10.3788/AOS231675

1 引 言

近年来，5G、云计算、大数据和自动驾驶等各种业务的快速发展，对光纤通信系统的传输容量提出了更高的要求。然而，传统的单模光纤的复用能力和速率提升已经到达了瓶颈期，其容量接近非线性香农极限[1]，无法满足不断增长的通信需求。为了解决这一问题，人们开始研究新的空分复用技术，其中模分复用(MDM)作为空分复用技术的重要组成部分，利用少模光纤中正交的模式作为独立的信道传输信号，可以成倍提升传输容量与频谱效率[2]。因此，MDM技术在光通信领域将具有广阔的前景，这也成为了当前光通信技术研究的热点之一。

多进多出(MIMO)均衡在MDM系统中一直扮演着关键的角色，特别是在处理模式串扰(XT)等损伤时具有显著的均衡效果[3]。2004年，Hsu等[4]研究了相干光通信中的MIMO均衡技术，将MIMO引入光纤通信中。2013年，He等[5]将MIMO均衡与频域最小均方(LMS)相结合，提出了改进的MIMO-FDE-LMS算法，将收敛速度提高了30%。2014年，van Uden等[6]搭建了三模双偏振相干传输实验装置，证明使用最小均方误差时域均衡器和频域均衡器(FDE)的收敛时间可以分别减少约50%和30%。2018年，He等[7]证明了MIMO中的递推最小二乘算法的收敛速度比传统频域LMS提高53.7%。2021年，Zou等[8]使用强度调制-直接检测的方式，结合查找表算法，在20 m标准OM2光纤上以1.6 Tbit/s的速率传输了3个模式。2023年，睢洲等[9]利用两个正交偏振及LP11a、LP11b两个模式，在最长达1000 km的少模光纤上传输32 GBaud的16QAM信号，系统实现的净速率为32.768 Tbit/s，属于国内领先水平。可以看出，由于光纤工艺和其他硬件的限制，相比于国外，国内进行的MDM相关实验中光纤模式较少，且长度较短，难以满足骨干网“超大容量、超长距离”的通信需求，但目前我国在MDM算法领域的研究发展迅速，处于追赶阶段。

MIMO均衡的系数设计与光纤模式之间的耦合系数有密切关系。为了解决模间信号XT的问题，使MIMO均衡更有效且具有针对性，研究模式耦合的机理变得尤为必要[10-11]。耦合模理论和功率耦合理论揭示了同一模场幅值的一阶导数与本模场和相邻模场的能量之间的联系，这种联系使得光场的幅度和相位相比于单模传输时都会发生变化[12-13]。此外，在实际传输系统中，相位噪声常以一种零均值随机过程的形式出现在XT中，这种随机性也给MIMO均衡的系数设计带来了新的挑战。因此，对于模式XT的深入研究可以提高MIMO均衡的效率和精度，使其在光通信系统中更加稳定和可靠[14]。传统检测方法基于物理测量给出的模式XT强度的表达式[15]只与接收端和发射端两处的功率相关，并不能体现链路中XT的随机性和周期性[16-17]，具有较大的局限性。

收稿日期：2023-10-19；**修回日期**：2023-11-30；**录用日期**：2023-12-21；**网络首发日期**：2023-12-23

基金项目：国家重点研发计划(2018YFB1800900，2020YFB1805805)、国家自然科学基金(62021005，62027817)、常州市重点研发计划(CE20225005)、装备预研教育部联合基金项目(8091B032133)

通信作者：*tianfeng@bupt.edu.cn

本文提出的多进多出恒模盲均衡算法(CPR-MIMO-CMA),结合接收端数字信号与发送信号的互相关函数,得到各模式间的XT-CPR,构造逆向MIMO传输矩阵,再使用可变步长因子的CMA对其系数进行迭代更新。XT-CPR直观反映了模式耦合对信号的综合影响程度,消除了随机性带来的误差,提升了MIMO均衡的针对性和准确性。搭建了两模光纤传输仿真平台和三模光纤传输实验平台,研究了XT-CPR的特征,得到了XT-CPR与XT强度、传输距离之间的关系,实验平台验证了该方法的可行性,证明了所提出的基于信号相关峰的MIMO-CMA均衡比传统CMA均衡具有明显的误码率性能提升,并且具有更快的收敛速度。

2　基本原理

2.1　模式耦合理论

理想情况下的波导的所有传播模式与辐射模式之间满足正交关系,各模式独立传播,模式间无能量交换。但在非理想的实际情况下,波导结构存在一定的不完整性,如波导的损耗、波导边界或几何形状有畸变、材料不均匀、波导周围存在其他波导、特意制作的波导结构的有规则的改变等,都会导致波导内模式间或波导之间的能量交换,这就是模式间耦合[10,12]。模式间耦合会导致不同模式间的能量受到相互影响,形成信号间的XT,从而降低信号的质量。

为了研究模式间耦合现象,需要对第u阶和第v阶模式间的耦合模方程以及耦合系数进行建模。首先,假设耦合模型中光场沿着坐标系z轴的正方向传播,x、y轴所在的平面即光纤截面所在的平面。截面上少模光纤的理想折射率分布为$n(x,y)$,与传播距离z无关。代入光纤波导结构所确定的边界条件,通过数值法求解波动方程,可以得到若干个满足导模条件的本征模式,记为$F_m(x,y)$,$m=1,2,\cdots$,这些模式相互正交,不会发生能量转移,对应了少模传输中的不同信道。光纤中的总光场可以用不同模式作为基本函数叠加得到[18]:

$$\tilde{\boldsymbol{E}}(x,y,z,\omega)=\sum_{m=1}^{M}\exp\left[\mathrm{i}\beta_m(\omega)z\right]\tilde{\boldsymbol{A}}_m(z,\omega)F_m(x,y),\tag{1}$$

式中:$\tilde{\boldsymbol{E}}$为光纤中各模式电场的总和;ω为角频率;M为一个发射周期内数字信号的数量;$\tilde{\boldsymbol{A}}_m(z,\omega)$为模式$m$在$z$方向上缓变复振幅矢量的傅里叶变换;$\beta_m$为模式$m$光信号的等效传播常数。

为了理论推导及模型计算的简化,假设光载波为准单色光,即忽略光频率的影响。当光纤的几何结构与折射率分布的扰动比较微小时,第u阶和第v阶模式间的耦合模方程以及耦合系数表达式[19-20]可以分别表示为

$$\frac{\partial A_u^+}{\partial z}=\sum C_{vu}A_v^+\exp\left[-\mathrm{j}(\beta_v-\beta_u)z\right],\tag{2}$$

$$C_{vu}=\frac{\boldsymbol{k}_0^2}{\mathrm{j}2\beta_u}\int_s\left[n(x,y,z)^2-n_0^2\right]\Psi_v^+\left(\Psi_u^+\right)^*\mathrm{d}s,\tag{3}$$

式中:A_v^+和A_u^+分别为模式v和模式u电场的缓变复振幅,右上角的正号表示两者的传播方向;$\boldsymbol{k}_0$为波矢;β_v和β_u分别为模式v和模式u的等效传播常数;Ψ_v^+和Ψ_u^+分别为模式v和模式u的场分布函数,在基于标量线偏振模的近似下,场分布函数都为实数,即$\Psi_u^{+*}=\Psi_u^+$;$n(x,y,z)$为光纤的折射率分布;n_0为理想光纤折射率分布;C_{vu}为模式v和模式u之间的耦合系数,它来源于光纤结构(即截面折射率分布)与标准结构的差异,当这种差异扰动较小时,可以认为发生了弱耦合[21],忽略光纤损耗,解微分方程得

$$A_u(z)=A_u(0)\exp(-\mathrm{j}\beta_u z)+C_{vu}\int_0^z A_v\exp\left[-\mathrm{j}(\beta_v-\beta_u)z\right]\mathrm{d}z。\tag{4}$$

可以看出,此时的u信道中包括了原A_u光信号和XT传递的A_v光信号两部分,其中XT强度随着耦合系数的改变而改变。

2.2　信号相关峰

如图1所示,发射端信号通过图1(a)所示的光纤链路后,得到图1(b)所示的错位信号。根据模式耦合理论,多路复用信号中的每一路信号都带有其他路的分量[22],在少模传输系统接收端,接收到的u路信号表达式为

$$s(t)=s_u(t)+ks_v(t),\tag{5}$$

式中:$s(t)$为实际接收到的信号,包括了原信号部分$s_u(t)$以及模式耦合部分$ks_v(t)$;系数k满足

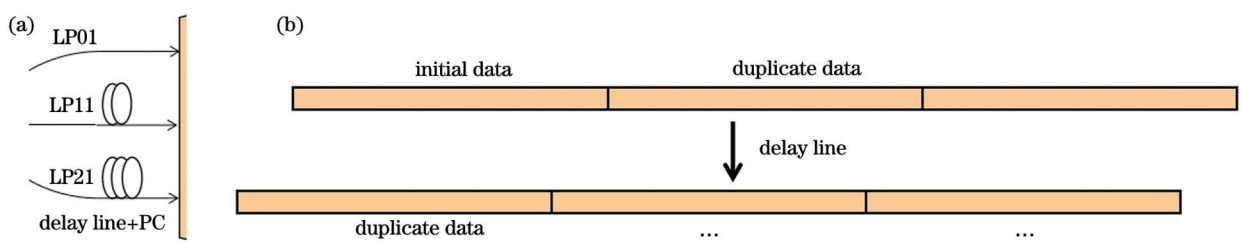

图1　重复数据错位发送。(a)光纤链路;(b)错位数据

Fig. 1　Duplicate data misplacement sending. (a) Fiber link; (b) unaligned data

$$k \propto C_{uv} \propto \int_{-\infty}^{+\infty}\int_{-\infty}^{+\infty}\left[n(x,y,z)^2-n_0^2\right]\Psi_v^+\left(\Psi_u^+\right)^* \mathrm{d}x\mathrm{d}y。 \tag{6}$$

对接收信号进行采样、滤波、时钟恢复等操作，得到数字信号序列$s(n)$，n为正整数。$s(n)$满足

$$s(n)=s_u(n)+ks_v(n), \tag{7}$$

式中：$s_u(n)$和$s_v(n)$分别为u信道和v信道中的数字信号序列。将$s(n)$与原始发射数据取互相关函数，数学表达式为

$$R_{s,s_{u0}}(\tau)=\frac{1}{M}\sum_{n=1}^{M}s(n)s_{u0}(n-\tau)+\frac{k}{M}\sum_{n=1}^{M}s_u(n)s_v(n-\tau), \tag{8}$$

式中：s_{u0}为u信道发射端的初始数据。由于信号是伪随机的，有且仅有唯一的$m_1\in[1,M]$，使得$\tau=m_1$时，$\int_1^M s_u(n)s_{u0}(n-\tau)\mathrm{d}n$取到最大值，即相关峰峰值。同理，有且仅有唯一的$m_2\in[1,M]$，使得$\tau=m_2$时，$\int_{n=1}^{M}s_u(n)s_v(n-\tau)\mathrm{d}n$取到最大值。$R_{s,s_{u0}}(\tau)$有两个峰值，其中一个来源于原信号，另外一个来源于XT信号，原信号峰值大于XT信号峰值，它们的比值即$C_{\mathrm{XT,CPR}}$：

$$C_{\mathrm{XT,CPR}}=\frac{\max\left[\sum_{n=1}^{M}s_u(n)s_{u0}(n-\tau)\right]}{\max\left[k\sum_{n=1}^{M}s_u(n)s_v(n-\tau)\right]}。 \tag{9}$$

为了进一步研究$C_{\mathrm{XT,CPR}}$与耦合系数的关系，利用OptiSystem15仿真软件搭建了少模传输平台，系统框图如图2所示，其中，①代表分段式[23]仿真模型，②代表掺铒光纤放大器（EDFA）、光学滤波器等其他光通信必要的器件。

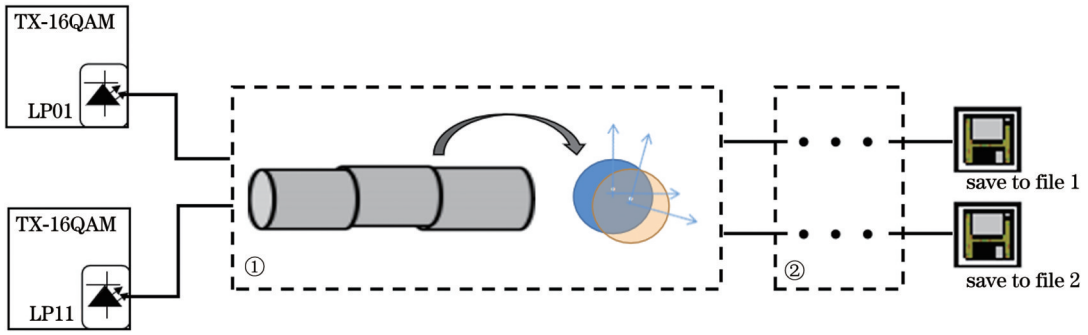

图2　两模耦合仿真框图

Fig. 2　Two mode coupling simulation diagram

发射端使用模式激光发生器产生LP01模和LP11模的光信号，光信号经过16QAM调制后进入少模光纤链路，对接收端的两路信号分别进行数字信号处理，求出$C_{\mathrm{XT,CPR}}$，并多次改变光纤长度和耦合强度，记录数据。图3为$C_{\mathrm{XT,CPR}}$与耦合强度、传播距离的关系图，其中，图3（a）中测试数据主要集中在每段光纤$0\sim5\times10^{-5}$的耦合强度范围内，可以看出，$C_{\mathrm{XT,CPR}}$随着耦合强度的增加呈现非线性下降的趋势，耦合强度较小时下降斜率较大，在耦合强度较大时下降趋势平缓；图3（b）中测试数据主要集中在30～80 km传播距离内，可以看出，$C_{\mathrm{XT,CPR}}$随着传播距离的增加呈现近似线性下降的趋势，在距离较远时下降趋势趋于平缓，这是由于此时光纤内的信号受到了严重的XT，XT信号的强度已经接近甚至超过本模式内信号强度。

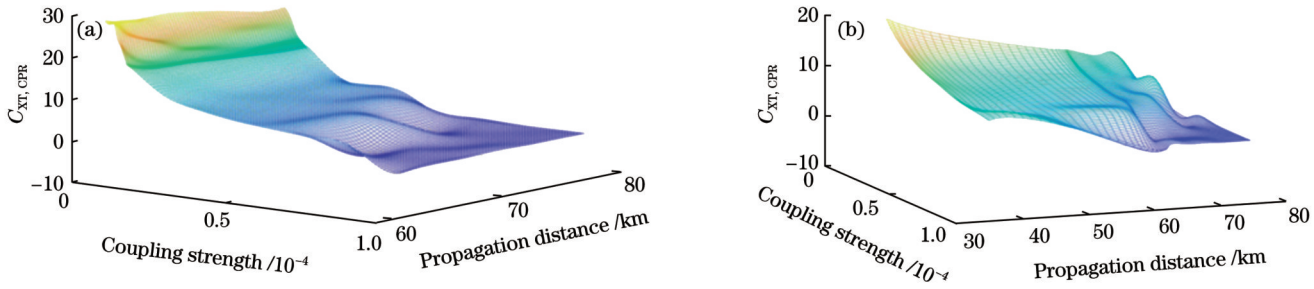

图3　$C_{\mathrm{XT,CPR}}$与耦合强度、传播距离的关系。（a）数据集中在低XT强度、大传播距离区；（b）数据集中在高XT强度区

Fig. 3　Relationship among $C_{\mathrm{XT,CPR}}$, coupling strength, and propagation distance. (a) Data is concentrated in areas with low XT intensity and large propagation distance; (b) data is concentrated in high XT intensity areas

2.3　CPR-MIMO-CMA

图4为本文所提出的基于信号相关峰的CPR-MIMO-CMA的流程图，其中，$s_1(n)$、$s_2(n)$、$s_3(n)$分别为待均衡的三路数字信号序列，$h_{ij}(i,j=1,2,3)$为

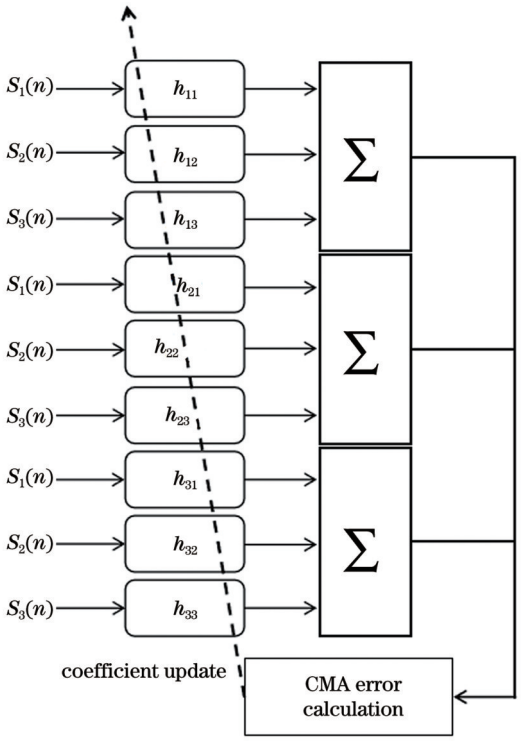

图 4　3×3 CPR-MIMO-CMA 流程图

Fig. 4　Flow chart of 3×3 CPR-MIMO-CMA

FIR(finite impulse response)滤波器组，该滤波器组共包含 9 个 FIR 滤波器，h_{ij} 也是 MIMO 矩阵的系数，在算法中该系数由梯度下降的方式进行更新。滤波器的长度与传输距离和模式间的差分模式群时延(DMGD)有关，当光纤长度较长或者 DMGD 较大时，h_{ij} 的长度可以适当增加[24]，本文所用 h_{ij} 的长度为 7。

为了简化运算，下面用 h_{ij} 来表示滤波器中心系数的值，其初值为 0。该流程主要包括两个部分。第一部分是 h_{ij} 初值的设定：

$$h_{ij}=\frac{1}{C_{\mathrm{XT,CPR}(ij)}},\tag{10}$$

式中：$C_{\mathrm{XT,CPR}(ij)}$ 为 i 路和 j 路之间的 $C_{\mathrm{XT,CPR}}$。第二部分是对 h_{ij} 进行更新，传统 CMA 作为基于高阶统计量的算法，最严重的缺点就是收敛速度慢，因为估计高阶统计量要比估计低阶统计量需要更多的观测数据，花费更多的时间[25]。此外，CMA 作为隐性的基于高阶统计量的算法，易于收敛到局部极小点，这时就不能充分地去除码间干扰[26]。本文所提出的基于信号相关峰的 CPR-MIMO-CMA 结合少模信道传播特征，减少 CMA 收敛所需的时间，更适合模式耦合损伤的应用场景。更新 h_{ij} 所用的步长因子 u_{ij}，更新后的步长因子 u'_{ij} 可以表示为

$$u'_{ij}=\frac{u_{ij}}{C_{\mathrm{XT,CPR}(ij)}}。\tag{11}$$

这样算法可以在 XT 较大时具有更快的收敛速度和更好的均衡效果。

3　实验验证

3.1　实验装置

为了验证 CPR-MIMO-CMA 性能，本文搭建了三模传输实验平台，系统框图如图 5 所示。

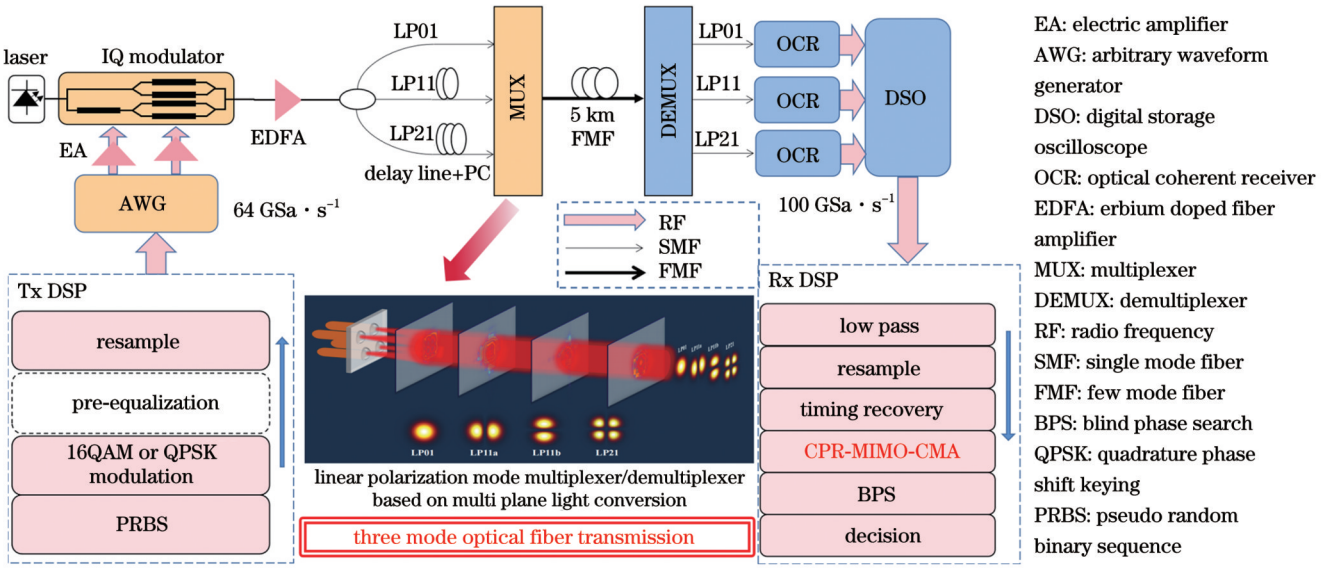

图 5　三模传输实验平台系统框图

Fig. 5　System block diagram of three mode transmission experimental platform

在发射端，首先通过 Matlab 生成码长为 2^{14} 的伪随机二进制序列，将其每 4 bit 映射成一个 16QAM 符号，通过根升余弦(RRC)滤波器来实现基带成型，信号经重采样后加载至采样率为 64 GSa/s 的任意波形发生器(AWG)，转换为两路电信号，用于驱动 IQ 调制器对两组光载波的调制，该 IQ 调制器的 3 dB 带宽为 29 GHz。激光器的工作波长为 1550.1 nm，调制后的光信号经过低噪声 EDFA 的放大后进入 1×3 耦合器。

同时，为了消除模式之间的相关性，将LP11路和LP21路光纤加入长度不同的延时线，并利用偏振控制器控制信号的偏振态。使用长度为5 km的阶跃型四模光纤，型号为FM SI-4，其模式耦合参数如表1所示。该光纤最多可以传输LP01、LP11a、LP11b、LP21这4个模式的光信号，本文采用其中LP01、LP11a、LP21 3个信道进行实验。

在接收端，复用信号被模式解复用器分为三路后进入相干接收机，观察并记录相关图像和波形数据，使用Matlab进行离线数字信号处理(DSP)。在DSP中，信号依次经过了RRC低通滤波器、重采样、时钟恢复以及本文提出的CPR-MIMO-CMA，然后通过盲相位搜索算法进入采样判决。

表1　FM SI-4的模式耦合参数

Table 1　Mode coupling parameters of FM SI-4

Mode	Mode crosstalk /dB			
	LP01	LP11a	LP11b	LP21
LP01	0	−21.90	−21.95	−28.46
LP11a	−21.90	0	−27.45	−26.32
LP11b	−21.95	−27.45	0	−25.23
LP21	−28.46	−26.32	−25.23	0

3.2　实验结果

对DSP信号与原始信号做互相关运算，相关峰$R_{s,s_{a0}}(\tau)$的图像如图6所示。

图6　三路信号中的相关峰。(a) LP01模式相关峰；(b) LP11a模式相关峰；(c) LP21模式相关峰

Fig. 6　Correlation peaks in three signals. (a) Correlation peak of LP01 mode; (b) correlation peak of LP11a mode; (c) correlation peak of LP21 mode

根据式(11)，其他条件一定时，XT越大，$C_{\mathrm{XT,CPR}}$越小，图6的相关峰高度对比与表1的参考数值所示的大小关系基本一致。

实验中采用低噪声EDFA将链路噪声维持在稳定且较小的范围内，改变信号的接收光功率，观察实验结果。图7为传统均衡与带CPR参数均衡下的误码率

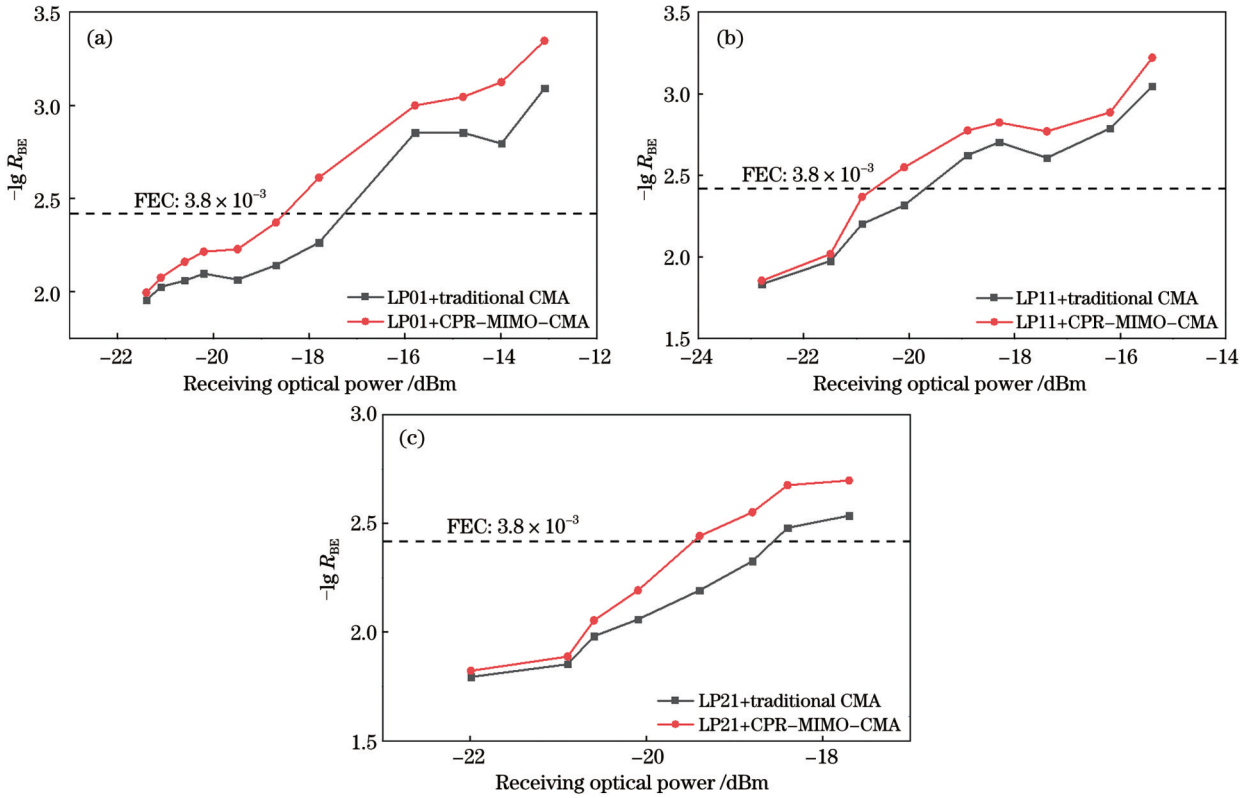

图7　3种模式下传统均衡与带CPR参数均衡的误码率与接收光功率的关系曲线。(a) LP01模式；(b) LP11模式；(c) LP21模式

Fig. 7　Relationship between error rate and received optical power of traditional equalization and equalization with CPR parameters in three modes. (a) LP01 mode; (b) LP11 mode; (c) LP21 mode

比较图，其中，R_{BE}为误码率。从图 7 中可以看出，在满足 FEC 为 3.8×10^{-3}的门限下，所提出的 CPR-MIMO-CMA 在 LP01、LP11、LP21 信道中比传统 CMA 分别具有 1.3 dB、0.9 dB、1.0 dB 的性能提升。在接收光功率较低即信噪比较大时，传统均衡与带 CPR 参数均衡的效果差别不大，这是由于此时噪声带来的损伤远大于模式 XT 所带来的损伤，在接收光功率较高时，带 CPR 参数的均衡效果达到最佳，随着接收光功率的不断增加，两者的均衡效果有接近的趋势，此时信号已经满足 FEC 为 3.8×10^{-3}的门限。

图 8 为 CPR-MIMO-CMA 与传统 CMA 处理三模传输系统接收端数据的平均收敛速度比较，从图 8 中可以看出，所提出的 CPR-MIMO-CMA 具有更快的收敛速度，3 个模式下的平均收敛时间减少约 50%。

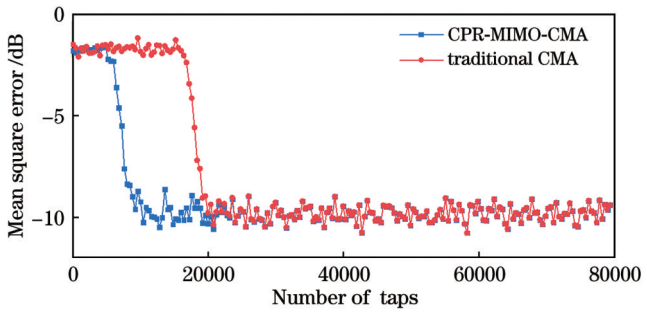

图 8　CPR-MIMO-CMA 与传统 CMA 的收敛速度比较

Fig. 8　Comparison of convergence speed between CPR-MIMO-CMA and traditional CMA

4　结　　论

提出了一种基于信号相关峰的 XT 均衡方法，该方法结合了模式耦合理论和信号相关峰理论，消除了传统衡量 XT 的随机性误差，使算法具有更好的模式均衡效果。搭建了三模传输实验平台，在实验平台上验证了该方法的可行性和准确性，比较了基于信号相关峰的 CPR-MIMO-CMA 与传统 CMA 均衡的误码率性能与收敛速度。结果表明，该方法能有效地均衡模式 XT，比传统均衡在 LP01、LP11、LP21 信道中分别具有 1.3 dB、0.9 dB、1.0 dB 的性能提升，并且 3 个模式下的平均收敛时间减少约 50%。

参　考　文　献

[1] 李博睿. 基于多芯光纤的空分复用光传输系统基础理论与关键技术研究[D]. 武汉: 华中科技大学, 2017.

[2] Su Y K, He Y, Chen H S, et al. Perspective on mode-division multiplexing[J]. Applied Physics Letters, 2021, 118(20): 200502.

[3] 何汶忠, 王晨, 王凯辉, 等. 8通道多维复用信号传输1000公里少模光纤[J]. 中文科技期刊数据库(全文版)自然科学, 2023(3): 1-4.
He W Z, Wang C, Wang K H, et al. 8-channel multi-dimensional multiplexing signal transmission with 1000 kilometers of low mode optical fiber[J]. Chinese Journal of Science and Technology Database (full text edition) Natural Science, 2023(3): 1-4

[4] Hsu R C J, Shah A, Jalali B. Coherent optical multiple-input multiple-output communication over multimode fiber[C]//2004 IEEE International Topical Meeting on Microwave Photonics, October 4-6, 2004, Ogunquit, ME, USA. New York: IEEE Press, 2005.

[5] He X, Zhou X, Wang J Y, et al. A fast convergence frequency domain least mean square algorithm for compensation of differential mode group delay in few mode fibers[C]//2013 Optical Fiber Communication Conference and Exposition and the National Fiber Optic Engineers Conference (OFC/NFOEC), March 17-21, 2013, Anaheim, CA. New York: IEEE Press, 2013.

[6] van Uden R G H, Okonkwo C M, Sleiffer V A J M, et al. MIMO equalization with adaptive step size for few-mode fiber transmission systems[J]. Optics Express, 2014, 22(1): 119-126.

[7] He X, Weng Y, Wang J Y, et al. Fast convergent frequency-domain MIMO equalizer for few-mode fiber communication systems[J]. Optics Communications, 2018, 409: 131-136.

[8] Zou D D, Li F, Wang W, et al. Beyond 1.6 Tb/s net rate PAM signal transmission for rack-rack optical interconnects with mode and wavelength division multiplexing[J]. Journal of Lightwave Technology, 2021, 39(2): 340-346.

[9] 睢洲, 王晨, 王凯辉, 等. 32.768 Tbit/s净速率1000 km长少模光纤波分复用系统[J]. 光学学报, 2023, 43(10): 1006004.
Ju Z, Wang C, Wang K H, et al. 1000-km-long few-mode fiber wavelength division multiplexing transmission system with net rate of 32.768 Tbit/s[J]. Acta Optica Sinica, 2023, 43(10): 1006004.

[10] Maruyama R, Kuwaki N, Matsuo S, et al. Relationship between mode coupling and fiber characteristics in few-mode fibers analyzed using impulse response measurements technique [J]. Journal of Lightwave Technology, 2017, 35(4): 650-657.

[11] Kubota H, Morioka T. Few-mode fibers for mode division multiplexing transmission[J]. Proceedings of SPIE, 2012, 8284: 82840E.

[12] Matthès M W, Bromberg Y, de Rosny J, et al. Learning and avoiding disorder in multimode fibers[J]. Physical Review X, 2021, 11(2): 021060.

[13] Mori T, Sakamoto T, Wada M, et al. Experimental verification of signal quality difference induced by differential modal loss and modal crosstalk on optical MIMO transmission and its compensation by equipartition multiplexing[J]. Journal of Lightwave Technology, 2016, 34(3): 918-927.

[14] 欧阳远江, 张倩武, 黄烨恬, 等. 基于MIMO预均衡的模分复用无源光网络模式间串扰的消除方法[J]. 中国激光, 2023, 50(6): 0606002.
Ouyang Y J, Zhang Q W, Huang Y T, et al. MIMO pre-equalization based mode crosstalk mitigation method in mode division multiplexing passive optical network[J]. Chinese Journal of Lasers, 2023, 50(6): 0606002.

[15] Liu F, He Z X, Zhang W P, et al. Mode dependent loss measurement of few mode fiber based on mode multiplexing power control[J]. IEEE Photonics Technology Letters, 2022, 34(3): 153-156.

[16] Rademacher G, Luís R S, Puttnam B J, et al. A comparative study of few-mode fiber and coupled-core multi-core fiber transmission[J]. Journal of Lightwave Technology, 2022, 40(6): 1590-1596.

[17] Zhang W P, Liu F, He Z X, et al. Fault detection performance of a multi-mode transmission reflection analysis for a few-mode fiber link[J]. Optics Letters, 2022, 47(1): 74-77.

[18] Koebele C, Salsi M, Charlet G, et al. Nonlinear effects in mode-division-multiplexed transmission over few-mode optical fiber[J]. IEEE Photonics Technology Letters, 2011, 23(18): 1316-1318.

[19] Gao X Y, Guo Y J, Shan W R. Optical waves/modes in a multicomponent inhomogeneous optical fiber via a three-coupled variable-coefficient nonlinear Schrödinger system[J]. Applied Mathematics Letters, 2021, 120: 107161.
[20] Fan X J, Wang D W, Cheng J L, et al. Few-mode fiber coupling efficiency for free-space optical communication[J]. Journal of Lightwave Technology, 2021, 39(6): 1823-1829.
[21] 张金玉, 任芳, 张艺赢, 等. 面向传感应用的弱耦合偏芯少模光纤设计与分析[J]. 光学学报, 2020, 40(24): 2406001.
Zhang J Y, Ren F, Zhang Y Y, et al. Design and analysis of weakly-coupled eccentric-core few-mode fiber for sensing application[J]. Acta Optica Sinica, 2020, 40(24): 2406001.
[22] Hanzawa N, Tsujikawa K, Kurokawa K, et al. Fiber fuse propagation characteristics of LP_{01} and LP_{11} modes in few-mode fiber[J]. Journal of Lightwave Technology, 2016, 34(15): 3628-3632.
[23] Juarez A A, Warm S, Bunge C A, et al. Perspectives of principal mode transmission in a multi-mode fiber[C]//36th European Conference and Exhibition on Optical Communication, September 19-23, 2010, Turin, Italy. New York: IEEE Press, 2010.
[24] 王健, 吴重庆. 低差分模式群时延少模光纤的变分法分析及优化[J]. 物理学报, 2022, 71(9): 094206.
Wang J, Wu C Q. Analysis and optimization of few-mode fibers with low differential mode group delay by variational method[J]. Acta Physica Sinica, 2022, 71(9): 094206.
[25] 杨绿溪. CMA 算法及在 MIMO 系统盲均衡中的应用[D]. 南京: 东南大学, 2003.
Yang L X. CMA algorithm and its application in blind equalization of MIMO systems[D]. Nanjing: Southeast University, 2003.
[26] 徐文婧, 李岩, 刘宇旸, 等. 相干光通信载波相位恢复算法研究[J]. 光学学报, 2021, 41(12): 1206002.
Xu W J, Li Y, Liu Y Y, et al. Carrier phase recovery algorithm for coherent optical communication[J]. Acta Optica Sinica, 2021, 41(12): 1206002.

CPR-MIMO-CMA in Mode Division Multiplexing Systems

Yang Bugao[1], Tian Feng[1*], Liu Xiaodong[2]

[1]*School of Electronic Engineering, State Key Laboratory of Information Photonics and Optical Communication, Beijing Key Laboratory of Space-Ground Interconnection and Convergence, Beijing University of Posts and Telecommunications, Beijing* 100876, *China*;

[2]*Beijing Ancoren Technology Co., Ltd, Beijing* 101102, *China*

Abstract

Objective With the rapid development of technologies such as the Internet and artificial intelligence, the demand for data in various fields of life is growing exponentially. However, the capacity of traditional single-mode fiber (SMF) networks is approaching the Shannon limit. Therefore, various multiplexing technologies including wavelength division multiplexing (WDM), polarization multiplexing (PDM), and mode division multiplexing (MDM) have been explored to meet the growing demand for data. In MDM, FMF fibers for long-distance transmission have lower nonlinear losses than multi-mode fibers, which makes it more cost-effective. Additionally, MDM introduces severe crosstalk among different modes, which should be compensated for by advanced DSP algorithms at the receiving end. We propose a crosstalk correlation ratio measurement method based on signal correlation peak extraction to address the channel crosstalk caused by mode coupling in MDM systems. The crosstalk correlation coefficient is applied to the correlation peak ratio multi-input-multi-output constant modulus algorithm (CPR-MIMO-CMA) to improve channel equalization performance. An SMF optic transmission experimental platform is built, and the CPR-MIMO-CMA is utilized to process the data from the receiving end to verify the algorithm superiority. The experimental results show that the proposed algorithm has a significant improvement in both convergence speed and balancing effect compared to traditional CMA, and is expected to be employed in future high-capacity FMF transmission scenarios.

Methods Firstly, we model and calculate the coupling mode equation and coupling coefficient, and derive the expression of the coupling coefficient in FMF and also the relationship between the signal correlation peak and it. Then, the FMF transmission system is built using simulation software. The signal generation end of the system is responsible for generating repetitive and misaligned digital signals. Then, the mode laser generator generates LP01 mode and LP11 mode optical signals, which are modulated by 16QAM and enter the FMF link. The FMF adopts a segmented simulation structure, and the two signals at the receiving end are processed with digital signals to obtain XT-CPR. It performs multiple changes in fiber length and coupling strength, recording data to explore the relationship among XT-CPR, coupling strength, and propagation distance. To verify the performance of the CPR-MIMO-CMA, we also build a third mock examination transmission experimental platform. At the transmitting end of the experimental system, firstly the software generates a pseudo-random binary sequence with a code length of 2^{14}, maps it into a 16QAM symbol every four

bits, and realizes baseband shaping through root raised cosine (RRC) filter. Meanwhile, the signal is loaded after resampling to an arbitrary waveform generator (AWG) with a sampling rate of 64 GSa/s, and it is converted into two electrical signals to drive the IQ modulator to modulate two groups of optical carriers. The 3 dB bandwidth of the IQ modulator is 29 GHz. The working wavelength of the laser is 1550.1 nm, and the modulated optical signal is amplified by a low noise erbium-doped fiber amplifier (EDFA) before entering a 1×3 coupler. At the same time, to eliminate the correlation between modes, we add LP11 and LP21 optical fibers with delay lines of different lengths and employ a polarization controller to control the polarization state of the signal. The fiber adopts a step type four-mode fiber with a length of 5 km, model FM SI-4, which can transmit up to four modes of optical signals including LP01, LP11a, LP11b, and LP21. Additionally, we employ three channels of LP01, LP11a, and LP21 for experiments. At the receiving end, the multiplexed signal is divided into three channels by the mode demultiplexer and enters the coherent receiver. The relevant image and waveform data are observed and recorded for offline digital signal processing (DSP). In the DSP, the signal is sequentially processed by the RRC low-pass filter, resampling, timing recovery, and the proposed CPR-MIMO-CMA. Then, the blind phase search algorithm is adopted to enter the sampling decision with experimental results observed.

Results and Discussions Fig. 6 shows a visual graph of the signal correlation peaks under three modes. According to Formula (11), when other conditions are constant, the larger crosstalk leads to smaller XT-CPR. The height comparison of the correlation peaks in Fig. 6 is basically consistent with the size relationship shown in the reference values of Table 1. Fig. 7 demonstrates a comparison of error rates between traditional equalization and equalization with CPR parameters. The figure indicates that the proposed CPR-MIMO-CMA has a performance improvement of 1.3 dB, 0.9 dB, and 1.0 dB compared to traditional CMA in LP01, LP11, and LP21 channels respectively under the threshold of forward error correction (FEC) of 3.8×10^{-3}. When the received optical power is low or the signal-to-noise ratio is high, there is not much difference in the effect between traditional equalization and equalization with CPR parameters. This is because the damage caused by noise is much greater than that caused by mode crosstalk. When the received optical power is high, the equalization effect with CPR parameters reaches the best. As the received optical power continues to increase, the equalization effect of the two tends to be similar. At this point, the signal already meets the FEC threshold of 3.8×10^{-3}. Fig. 8 shows a comparison of the average convergence speed of CPR-MIMO-CMA and the traditional CMA for processing the data at the receiving end of the third mock examination transmission system. This figure reveals that the proposed CPR-MIMO-CMA has a faster convergence speed, and the average convergence time under the three modes is reduced by about 50%.

Conclusions We propose a crosstalk equalization method based on signal correlation peaks, which combines mode coupling theory and signal correlation peak theory to eliminate the randomness error of traditional crosstalk measurement, making the algorithm have a better mode equalization effect. A third mock examination transmission experimental platform is built, on which the feasibility and accuracy of the method are verified. The BER performance and convergence speed of CPR-MIMO-CMA based on signal correlation peak and traditional CMA equalization are compared. The results show that the method can effectively equalize mode crosstalk, and the performance of this method is improved by 1.3 dB, 0.9 dB, and 1.0 dB respectively compared with traditional equalization in LP01, LP11, and LP21 channels. Meanwhile, the average convergence time in the three modes is reduced by about 50%.

Key words optical communications; mode division multiplexing; intermodal crosstalk; signal correlation peak; mode equalization